Immunity, Volume *49*

Supplemental Information

An Interleukin-23-Interleukin-22 Axis Regulates Intestinal Microbial Homeostasis to Protect from Diet-Induced Atherosclerosis

Aliia R. Fatkhullina, Iuliia O. Peshkova, Amiran Dzutsev, Turan Aghayev, John A. McCulloch, Vishal Thovarai, Jonathan H. Badger, Ravi Vats, Prithu Sundd, Hsin-Yao Tang, Andrew V. Kossenkov, Stanley L. Hazen, Giorgio Trinchieri, Sergei I. Grivennikov, and Ekaterina K. Koltsova

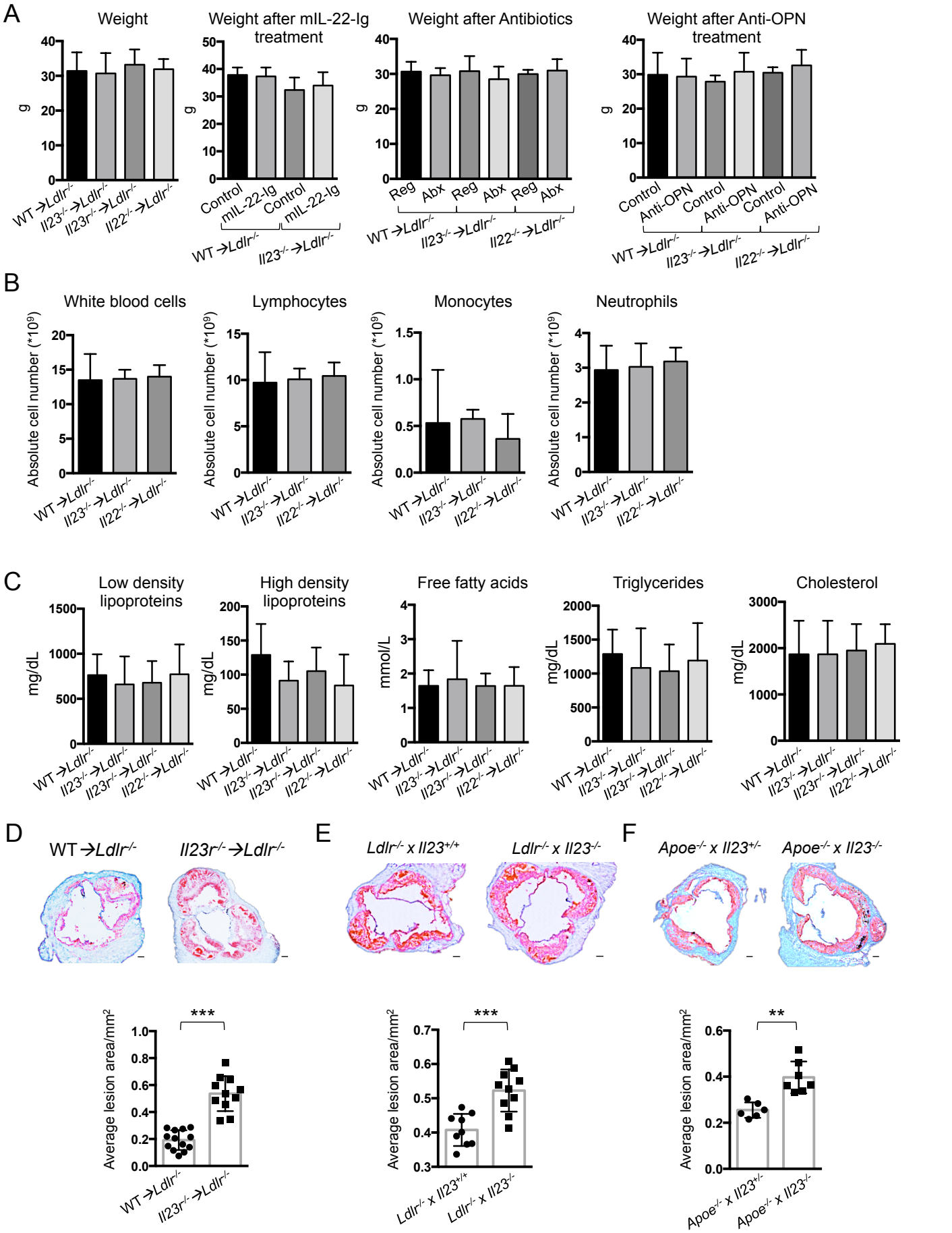
A
Weight
Weight after mIL-22-Ig treatment
Weight after Antibiotics
Weight after Anti-OPN treatment
g
WT →Ldlr-/-
Il23-/- →Ldlr-/-
Il23r-/- →Ldlr-/-
Il22-/- →Ldlr-/-
Control
mIL-22-Ig
Reg
Abx
Anti-OPN
B
White blood cells
Lymphocytes
Monocytes
Neutrophils
Absolute cell number (*10^9)
C
Low density lipoproteins
High density lipoproteins
Free fatty acids
Triglycerides
Cholesterol
mg/dL
mmol/L
D
WT →Ldlr-/-
Il23r-/- →Ldlr-/-
E
Ldlr-/- x Il23+/+
Ldlr-/- x Il23-/-
F
Apoe-/- x Il23+/-
Apoe-/- x Il23-/-
Average lesion area/mm2
***
**

Figure S1.

Figure S1. IL-23 and IL-22 pathway inactivation promotes atherosclerosis but does not affect body weight, blood cell count and serum lipid profile. Related to Figure 1.

A. Body weight of WT→*Ldlr*$^{-/-}$, *Il23r*$^{-/-}$→*Ldlr*$^{-/-}$ *Il23*$^{-/-}$→*Ldlr*$^{-/-}$ or *Il22*$^{-/-}$→*Ldlr*$^{-/-}$ mice after 16 weeks on Western diet (WD) (n=5-10 mice per group) in all conditions: mIL-22-Ig, antibiotic, anti-OPN treatments. **B.** Blood cell count in WT→*Ldlr*$^{-/-}$, *Il23*$^{-/-}$→*Ldlr*$^{-/-}$ or *Il22*$^{-/-}$→*Ldlr*$^{-/-}$ mice after 16 weeks on WD (n=5-10 mice per group). **C.** Serum triglyceride, high-density lipoprotein (HDL), low-density lipoprotein (LDL) and total cholesterol levels in WT→*Ldlr*$^{-/-}$ (n=5), *Il23*$^{-/-}$→*Ldlr*$^{-/-}$ (n=5), *Il23r*$^{-/-}$→*Ldlr*$^{-/-}$ (n=5) or *Il22*$^{-/-}$→*Ldlr*$^{-/-}$ (n=7) mice. **D**. Representative images of aortic root sections and quantitative comparison of atherosclerotic lesion size of WT→*Ldlr*$^{-/-}$ (n=13) or *Il23r*$^{-/-}$ →*Ldlr*$^{-/-}$ (n=11) mice fed with WD for 16 weeks. **E.** Representative images of aortic root sections and quantitative comparison of atherosclerotic lesion size of *Ldlr*$^{-/-}$ *x Il23*$^{+/+}$ (n=8) or *Ldlr*$^{-/-}$ *x Il23*$^{-/-}$ (n=9) mice fed with WD for 16 weeks. **F.** Representative images of aortic root sections and quantitative comparison of atherosclerotic lesion size of *Apoe*$^{-/-}$ *x Il23*$^{+/-}$ (n=6) or *Apoe*$^{-/-}$ *x Il23*$^{-/-}$ (n=7) mice fed with WD for 14 weeks. Scale bar represents 100μm. Data are mean ± SEM from 3 independent experiments. **p<0.001, ***p<0.0001.

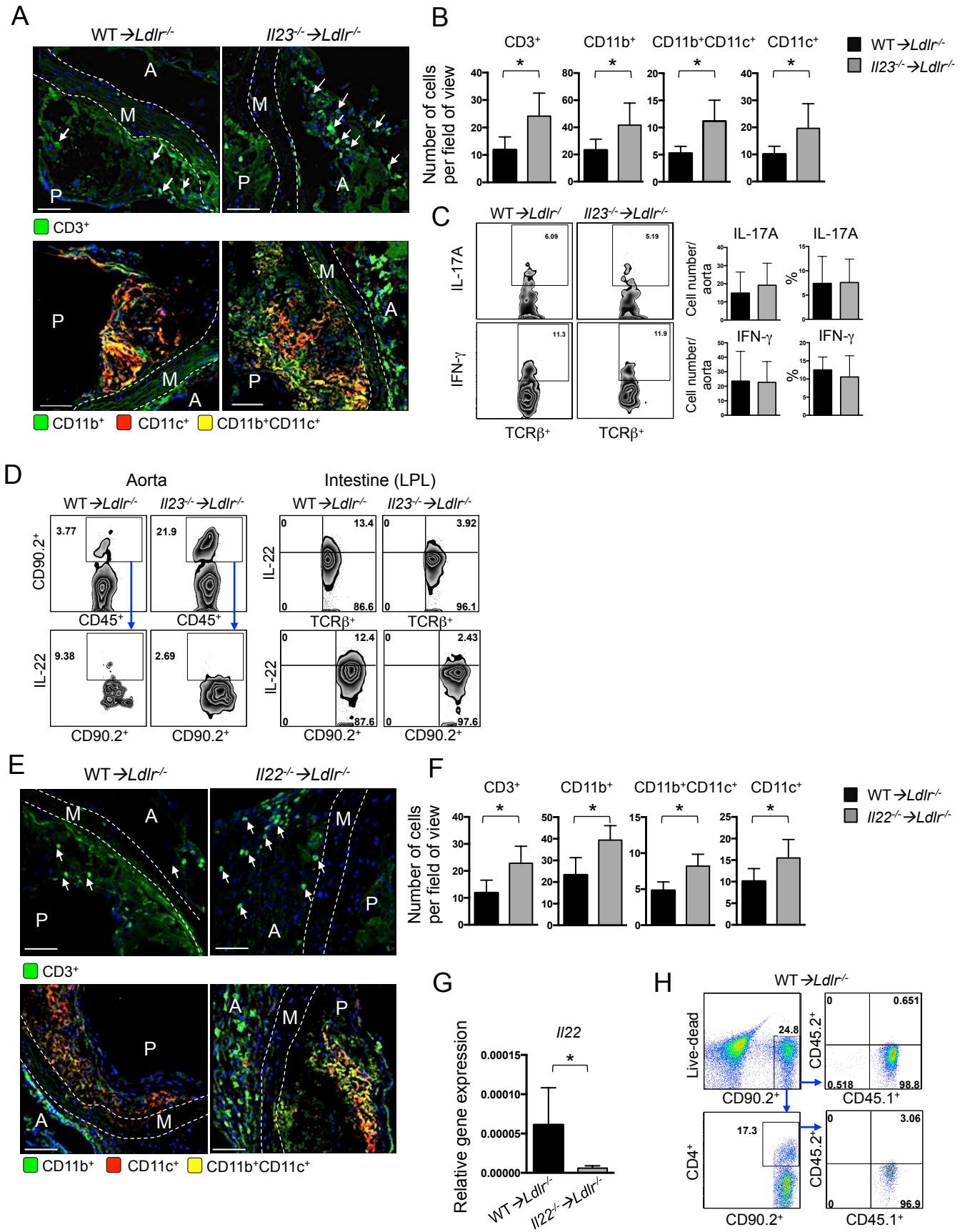
A
WT→Ldlr-/-
Il23-/-→Ldlr-/-
M
A
P
CD3+
CD11b+
CD11c+
CD11b+CD11c+
B
CD3+
CD11b+
CD11b+CD11c+
CD11c+
Number of cells per field of view
WT→Ldlr-/-
Il23-/-→Ldlr-/-
C
IL-17A
IFN-γ
TCRβ+
Cell number/ aorta
%
D
Aorta
Intestine (LPL)
CD90.2+
CD45+
TCRβ+
IL-22
E
Il22-/-→Ldlr-/-
F
G
Il22
Relative gene expression
H
Live-dead
CD45.2+
CD45.1+
CD4+

Figure S2.

Figure S2. Changes in immune cells accumulation and cytokine expression in *Il23*$^{-/-}$ →*Ldlr*$^{-/-}$, *Il22*$^{-/-}$→*Ldlr*$^{-/-}$ and WT→*Ldlr*$^{-/-}$ mice. Related to Figure 1 and 2.

A. Immunofluorescent analysis of aortic root sections. Localization of $CD3^+$ T cells and $CD11b^+$, $CD11b^+CD11c^+$, $CD11c^+$ myeloid cells in aortic roots of WT→*Ldlr*$^{-/-}$ or *Il23*$^{-/-}$→*Ldlr*$^{-/-}$ mice. Arrows show the localization of $CD3^+$ T cells. Representative images from 3 independent experiments. **B.** Quantification of immune cells in aortic roots of WT→*Ldlr*$^{-/-}$ or *Il23*$^{-/-}$→*Ldlr*$^{-/-}$ mice. **C.** Intracellular IFN-γ and IL-17A staining (gated on TCRβ) of T cells isolated from aortas of WT→*Ldlr*$^{-/-}$ or *Il23*$^{-/-}$→*Ldlr*$^{-/-}$ mice **(left panel);** cell number and percentage of IFN-γ and IL-17A producing T cells **(right panel). D** Intracellular IL-22 staining in T cells (gated on TCRβ) and innate lymphoid cells (gated on CD90.2) isolated from aorta and lamina propria (LPL) of WT→*Ldlr*$^{-/-}$ and *Il23*$^{-/-}$→*Ldlr*$^{-/-}$ mice. **E.** Immunofluorescent analysis of aortic root sections. Localization of $CD3^+$ T cells and $CD11b^+$, $CD11b^+CD11c^+$, $CD11c^+$ myeloid cells in aortic roots of WT→*Ldlr*$^{-/-}$ or *Il22*$^{-/-}$→*Ldlr*$^{-/-}$ mice. Arrows show the localization of $CD3^+$ T cells. Representative images from 3 independent experiments. **F.** Quantification of immune cells in aortic roots of WT→*Ldlr*$^{-/-}$ or *Il22*$^{-/-}$→*Ldlr*$^{-/-}$ mice**. G.** Relative *Il22* gene expression normalized to *RpL32* gene expression in the intestines of WT→*Ldlr*$^{-/-}$ (n=6) and *Il22*$^{-/-}$→*Ldlr*$^{-/-}$ (n=6). **H.** Reconstitution efficiency of ILC and T cells in intestine of mice after bone marrow transplantation**.** Data are mean ± SEM *$p<0.05$. Scale bar represents 50μm. A-adventitia, M-media, P-plaque.

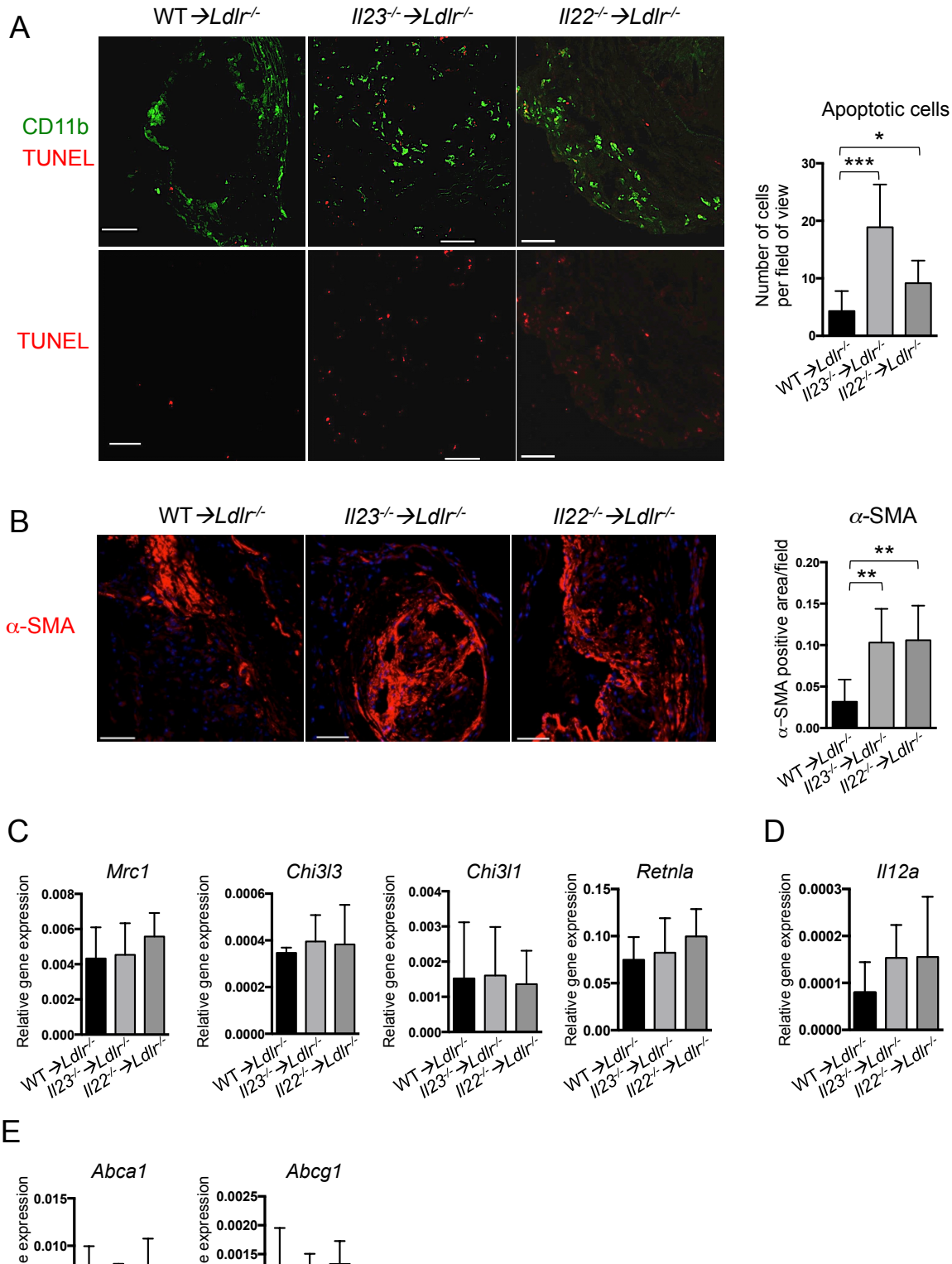
A
WT→Ldlr-/-
Il23-/-→Ldlr-/-
Il22-/-→Ldlr-/-
CD11b
TUNEL
TUNEL
Apoptotic cells
Number of cells per field of view
B
α-SMA
α-SMA
α-SMA positive area/field
C
Mrc1
Chi3l3
Chi3l1
Retnla
Relative gene expression
D
Il12a
Il12b
E
Abca1
Abcg1

Figure S3.

Figure S3. Macrophage related gene expression, apoptosis and smooth muscle cell proliferation in aortas of WT→*Ldlr*$^{-/-}$, *Il23*$^{-/-}$→*Ldlr*$^{-/-}$ and *Il22*$^{-/-}$→*Ldlr*$^{-/-}$ mice. Related to Figure 1 and 2.

A-C. IL-23 and IL-22 deficiency results in increased number of apoptotic cells and smooth muscle actin (α-SMA) in the aortic roots**. A.** TUNEL and Immunofluorescence analyzes, localization and quantification of apoptotic cells and CD11b^{+} macrophages in the aortic roots of WT→*Ldlr*$^{-/-}$, *Il23*$^{-/-}$→*Ldlr*$^{-/-}$ or *Il22*$^{-/-}$→*Ldlr*$^{-/-}$ mice. **B.** Immunofluorescence analysis and quantification of α-SMA in the aortic roots of WT→*Ldlr*$^{-/-}$, *Il23*$^{-/-}$→*Ldlr*$^{-/-}$ or *Il22*$^{-/-}$→*Ldlr*$^{-/-}$ mice. Representative images from 3 independent experiments. Scale bar represents 50μm. **C, D.** The expression of macrophage genes in the aorta of WT→*Ldlr*$^{-/-}$, *Il23*$^{-/-}$→*Ldlr*$^{-/-}$ or *Il22*$^{-/-}$→*Ldlr*$^{-/-}$ mice. **E.** Relative gene expression of cholesterol reverse transporters in the aorta of WT→*Ldlr*$^{-/-}$, *Il23*$^{-/-}$→*Ldlr*$^{-/-}$ or *Il22*$^{-/-}$→*Ldlr*$^{-/-}$ mice. Gene expression was normalized to *RpL32* gene expression. Data are mean ± SEM *p<0.05, **p<0.001, ***p<0.0001.

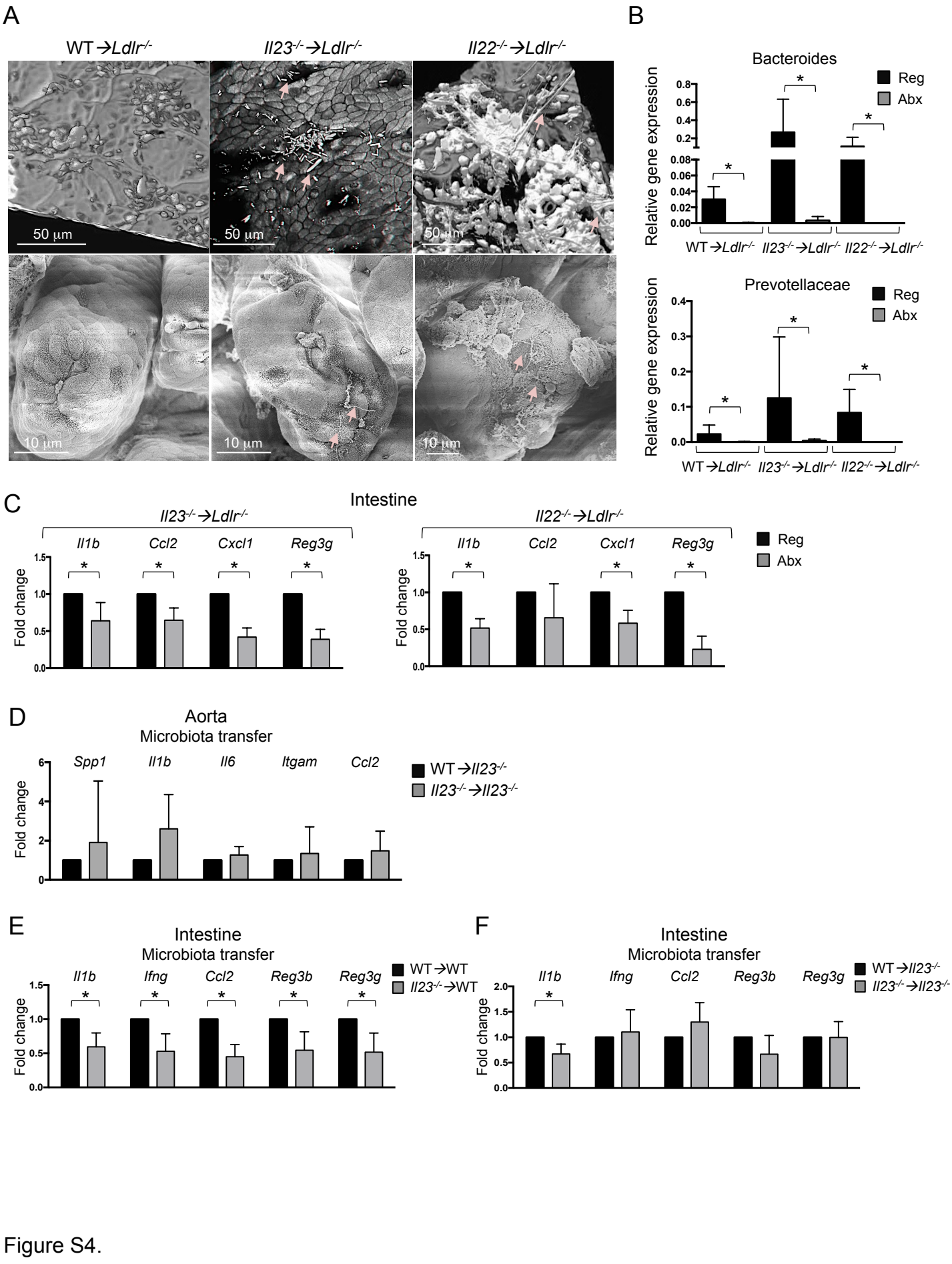
A
WT→Ldlr-/-
Il23-/-→Ldlr-/-
Il22-/-→Ldlr-/-
50 μm
10 μm
B
Bacteroides
Prevotellaceae
Relative gene expression
Reg
Abx
WT→Ldlr-/-
Il23-/-→Ldlr-/-
Il22-/-→Ldlr-/-
C
Intestine
Il23-/-→Ldlr-/-
Il22-/-→Ldlr-/-
Il1b
Ccl2
Cxcl1
Reg3g
Fold change
D
Aorta
Microbiota transfer
Spp1
Il1b
Il6
Itgam
Ccl2
WT→Il23-/-
Il23-/-→Il23-/-
E
Intestine
Microbiota transfer
Il1b
Ifng
Ccl2
Reg3b
Reg3g
WT→WT
Il23-/-→WT
F
Intestine
Microbiota transfer
WT→Il23-/-
Il23-/-→Il23-/-

Figure S4.

Figure S4. Cytokine alterations modulate microbiota localization and inflammatory gene expression. Related to Figure 3 and 4.

A. Representative images of whole mount intestine tissue from WT→*Ldlr*$^{-/-}$, *Il23*$^{-/-}$→*Ldlr*$^{-/-}$ or *Il22*$^{-/-}$→*Ldlr*$^{-/-}$ mice stained with YoYo dye of bacterial and host DNA (**top panel)** and scanning electron microscopy (SEM) of terminal ileum **(bottom panel).** Representative images from 2 independent experiments. **B.** Relative gene expression of *Prevotellaceae* and *Bacteroides* in the intestinal tissue of WT→*Ldlr*$^{-/-}$, *Il23*$^{-/-}$→*Ldlr*$^{-/-}$ or *Il22*$^{-/-}$→*Ldlr*$^{-/-}$ mice maintained on antibiotic-containing (Abx) or regular water (Reg); n=5-6. Gene expression was normalized to *RpL32* gene expression. **C.** Relative gene expression in the intestines of *Il23*$^{-/-}$→*Ldlr*$^{-/-}$ or *Il22*$^{-/-}$→*Ldlr*$^{-/-}$ mice maintained on antibiotic containing (Abx) or regular water (Reg). **D.** Relative gene expression in the aortas of *Il23*$^{-/-}$→*Ldlr*$^{-/-}$ mice received microbiota from WT→*Ldlr*$^{-/-}$ or *Il23*$^{-/-}$→*Ldlr*$^{-/-}$ atherosclerotic mice. **E.** Relative gene expression in the intestines of WT→*Ldlr*$^{-/-}$ mice received microbiota from WT→*Ldlr*$^{-/-}$ and *Il23*$^{-/-}$→*Ldlr*$^{-/-}$ atherosclerotic mice **F.** Relative gene expression in the intestines of *Il23*$^{-/-}$→*Ldlr*$^{-/-}$ mice received microbiota from WT→*Ldlr*$^{-/-}$ or *Il23*$^{-/-}$→*Ldlr*$^{-/-}$ atherosclerotic mice. **C-F.** Gene expression was normalized to *RpL32* gene expression and then normalized to average gene expression in the control group. Data are mean ± SEM from 3 independent experiments, *p<0.05.

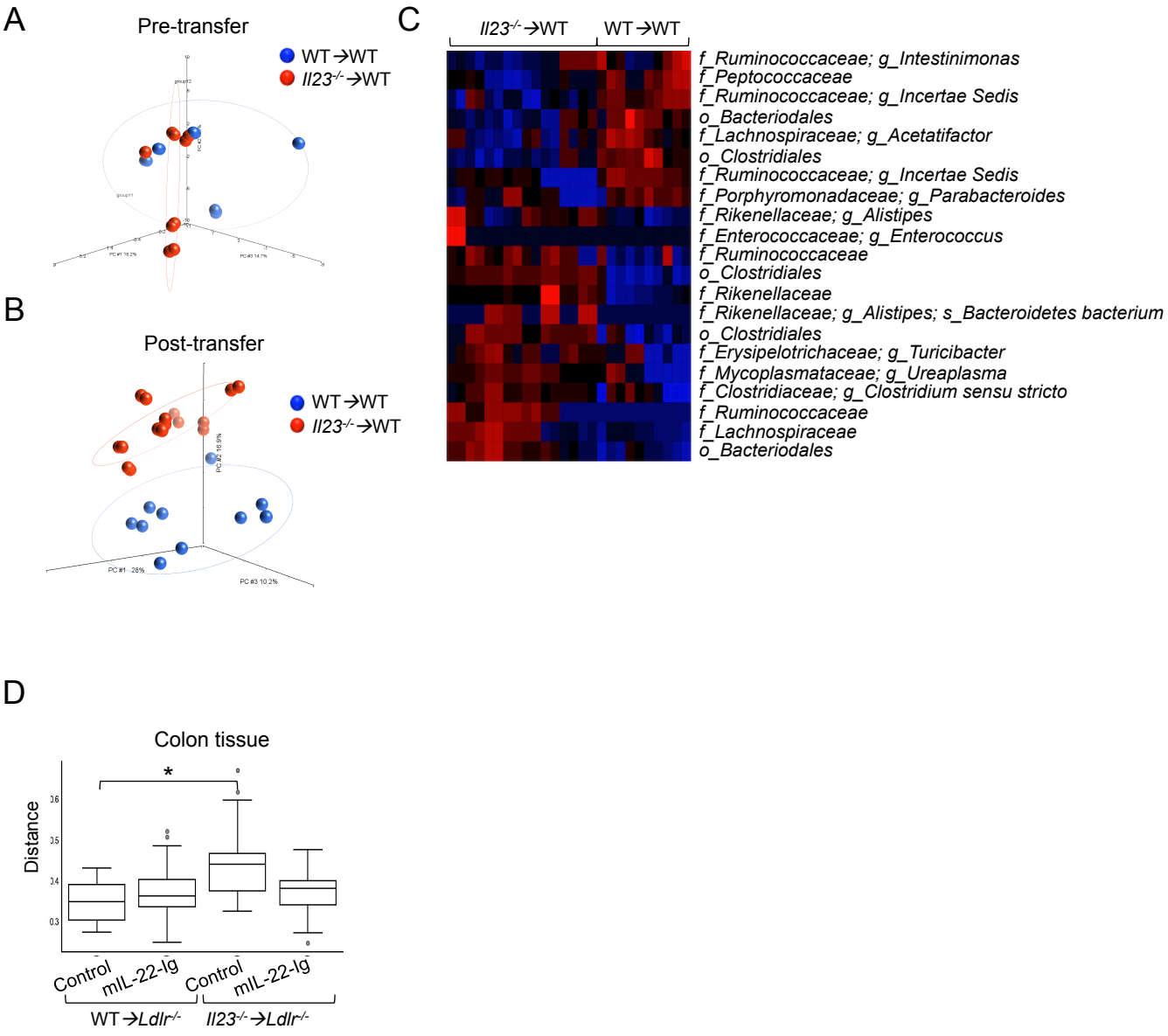
A
Pre-transfer
WT→WT
Il23-/-→WT
B
Post-transfer
WT→WT
Il23-/-→WT
C
Il23-/-→WT
WT→WT
f_Ruminococcaceae; g_Intestinimonas
f_Peptococcaceae
f_Ruminococcaceae; g_Incertae Sedis
o_Bacteriodales
f_Lachnospiraceae; g_Acetatifactor
o_Clostridiales
f_Ruminococcaceae; g_Incertae Sedis
f_Porphyromonadaceae; g_Parabacteroides
f_Rikenellaceae; g_Alistipes
f_Enterococcaceae; g_Enterococcus
f_Ruminococcaceae
o_Clostridiales
f_Rikenellaceae
f_Rikenellaceae; g_Alistipes; s_Bacteroidetes bacterium
o_Clostridiales
f_Erysipelotrichaceae; g_Turicibacter
f_Mycoplasmataceae; g_Ureaplasma
f_Clostridiaceae; g_Clostridium sensu stricto
f_Ruminococcaceae
f_Lachnospiraceae
o_Bacteriodales

D
Colon tissue
*
Distance
0.6
0.5
0.4
0.3
Control
mIL-22-Ig
Control
mIL-22-Ig
WT→Ldlr-/-
Il23-/-→Ldlr-/-

Figure S5.

Figure S5. Microbiome alterations are dependent of IL-23 and IL-22 cytokines. Related to Figure 4.

A. Principal component analysis of the cecum luminal microbiota of WT→*Ldlr*$^{-/-}$ mice (recipients of microbiota from WT→*Ldlr*$^{-/-}$ (blue) or *Il23*$^{-/-}$→*Ldlr*$^{-/-}$ (red) donors) before microbiome transplantation. Principal component analysis **(B)** and heat map **(C)** of the cecum luminal microbiota of WT→*Ldlr*$^{-/-}$ mice after microbiome transfer from atherosclerotic WT→*Ldlr*$^{-/-}$ or *Il23*$^{-/-}$→*Ldlr*$^{-/-}$ followed by WD feeding for 16 weeks. Red – upregulated bacteria, blue – downregulated bacteria. **D**. Global microbiome comparison in WT→*Ldlr*$^{-/-}$ and *Il23*$^{-/-}$→*Ldlr*$^{-/-}$ mice administered with mIL-22-Ig or control. *p<0.05.

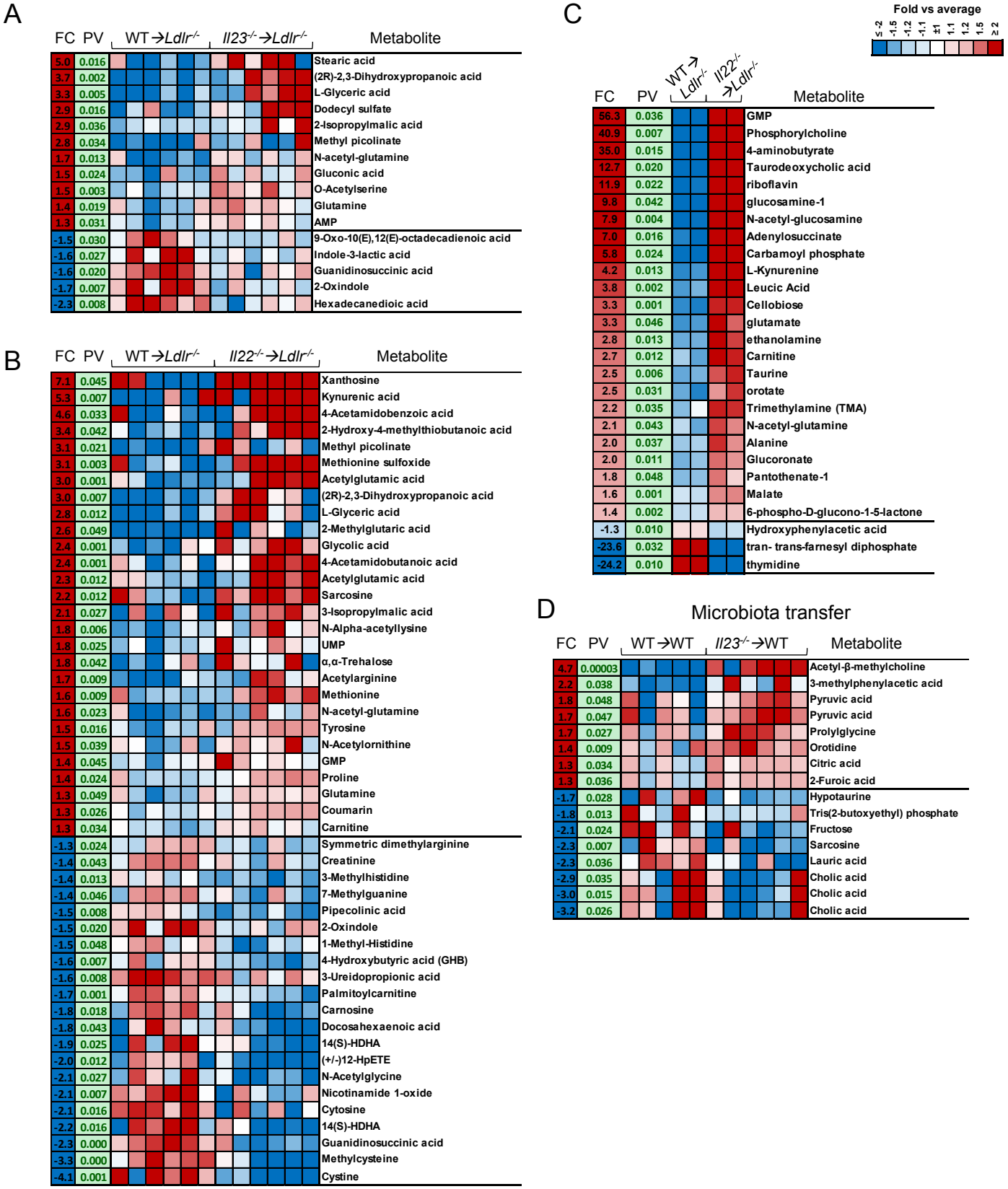
A
FC PV WT→Ldlr-/- Il23-/-→Ldlr-/- Metabolite
5.0 0.016 Stearic acid
3.7 0.002 (2R)-2,3-Dihydroxypropanoic acid
3.3 0.005 L-Glyceric acid
2.9 0.016 Dodecyl sulfate
2.9 0.036 2-Isopropylmalic acid
2.8 0.034 Methyl picolinate
1.7 0.013 N-acetyl-glutamine
1.5 0.024 Gluconic acid
1.5 0.003 O-Acetylserine
1.4 0.019 Glutamine
1.3 0.031 AMP
-1.5 0.030 9-Oxo-10(E),12(E)-octadecadienoic acid
-1.6 0.027 Indole-3-lactic acid
-1.6 0.020 Guanidinosuccinic acid
-1.7 0.007 2-Oxindole
-2.3 0.008 Hexadecanedioic acid
B
FC PV WT→Ldlr-/- Il22-/-→Ldlr-/- Metabolite
7.1 0.045 Xanthosine
5.3 0.007 Kynurenic acid
4.6 0.033 4-Acetamidobenzoic acid
3.4 0.042 2-Hydroxy-4-methylthiobutanoic acid
3.1 0.021 Methyl picolinate
3.1 0.003 Methionine sulfoxide
3.0 0.001 Acetylglutamic acid
3.0 0.007 (2R)-2,3-Dihydroxypropanoic acid
2.8 0.012 L-Glyceric acid
2.6 0.049 2-Methylglutaric acid
2.4 0.001 Glycolic acid
2.4 0.001 4-Acetamidobutanoic acid
2.3 0.012 Acetylglutamic acid
2.2 0.012 Sarcosine
2.1 0.027 3-Isopropylmalic acid
1.8 0.006 N-Alpha-acetyllysine
1.8 0.025 UMP
1.8 0.042 α,α-Trehalose
1.7 0.009 Acetylarginine
1.6 0.009 Methionine
1.6 0.023 N-acetyl-glutamine
1.5 0.016 Tyrosine
1.5 0.039 N-Acetylornithine
1.4 0.045 GMP
1.4 0.024 Proline
1.3 0.049 Glutamine
1.3 0.026 Coumarin
1.3 0.034 Carnitine
-1.3 0.024 Symmetric dimethylarginine
-1.4 0.043 Creatinine
-1.4 0.013 3-Methylhistidine
-1.4 0.046 7-Methylguanine
-1.5 0.008 Pipecolinic acid
-1.5 0.020 2-Oxindole
-1.5 0.048 1-Methyl-Histidine
-1.6 0.007 4-Hydroxybutyric acid (GHB)
-1.6 0.008 3-Ureidopropionic acid
-1.7 0.001 Palmitoylcarnitine
-1.8 0.018 Carnosine
-1.8 0.043 Docosahexaenoic acid
-1.9 0.025 14(S)-HDHA
-2.0 0.012 (+/-)12-HpETE
-2.1 0.027 N-Acetylglycine
-2.1 0.007 Nicotinamide 1-oxide
-2.1 0.016 Cytosine
-2.2 0.016 14(S)-HDHA
-2.3 0.000 Guanidinosuccinic acid
-3.3 0.000 Methylcysteine
-4.1 0.001 Cystine
C
Fold vs average
≤ -2 -1.5 -1.2 -1.1 ±1 1.1 1.2 1.5 ≥ 2
FC PV WT→Ldlr-/- Il22-/-→Ldlr-/- Metabolite
56.3 0.036 GMP
40.9 0.007 Phosphorylcholine
35.0 0.015 4-aminobutyrate
12.7 0.020 Taurodeoxycholic acid
11.9 0.022 riboflavin
9.8 0.042 glucosamine-1
7.9 0.004 N-acetyl-glucosamine
7.0 0.016 Adenylosuccinate
5.8 0.024 Carbamoyl phosphate
4.2 0.013 L-Kynurenine
3.8 0.002 Leucic Acid
3.3 0.001 Cellobiose
3.3 0.046 glutamate
2.8 0.013 ethanolamine
2.7 0.012 Carnitine
2.5 0.006 Taurine
2.5 0.031 orotate
2.2 0.035 Trimethylamine (TMA)
2.1 0.043 N-acetyl-glutamine
2.0 0.037 Alanine
2.0 0.011 Glucoronate
1.8 0.048 Pantothenate-1
1.6 0.001 Malate
1.4 0.002 6-phospho-D-glucono-1-5-lactone
-1.3 0.010 Hydroxyphenylacetic acid
-23.6 0.032 tran- trans-farnesyl diphosphate
-24.2 0.010 thymidine
D
Microbiota transfer
FC PV WT→WT Il23-/-→WT Metabolite
4.7 0.00003 Acetyl-β-methylcholine
2.2 0.038 3-methylphenylacetic acid
1.8 0.048 Pyruvic acid
1.7 0.047 Pyruvic acid
1.7 0.027 Prolylglycine
1.4 0.009 Orotidine
1.3 0.034 Citric acid
1.3 0.036 2-Furoic acid
-1.7 0.028 Hypotaurine
-1.8 0.013 Tris(2-butoxyethyl) phosphate
-2.1 0.024 Fructose
-2.3 0.007 Sarcosine
-2.3 0.036 Lauric acid
-2.9 0.035 Cholic acid
-3.0 0.015 Cholic acid
-3.2 0.026 Cholic acid

Figure S6.

Figure S6. Alteration of serum metabolites in IL-23 and IL-22 deficient atherosclerotic mice. Related to Figure 5.

Heat map of serum metabolites of WT→*Ldlr*$^{-/-}$ and *Il23*$^{-/-}$→*Ldlr*$^{-/-}$ **(A)** or WT→*Ldlr*$^{-/-}$ and *Il22*$^{-/-}$→*Ldlr*$^{-/-}$ mice **(B)** fed with WD for 16 weeks. **C.** Heat map of serum metabolites of WT→*Ldlr*$^{-/-}$ and *Il22*$^{-/-}$→*Ldlr*$^{-/-}$ mice fed with WD+1% choline for 16 weeks. **D.** Heat map of serum metabolites of WT→*Ldlr*$^{-/-}$ mice that received the microbiota from WT→*Ldlr*$^{-/-}$ or *Il23*$^{-/-}$→*Ldlr*$^{-/-}$ atherosclerotic donors. Red – upregulated metabolites, blue – downregulated metabolites, FC-fold change. Representative data from 2 independent metabolomics analyses.

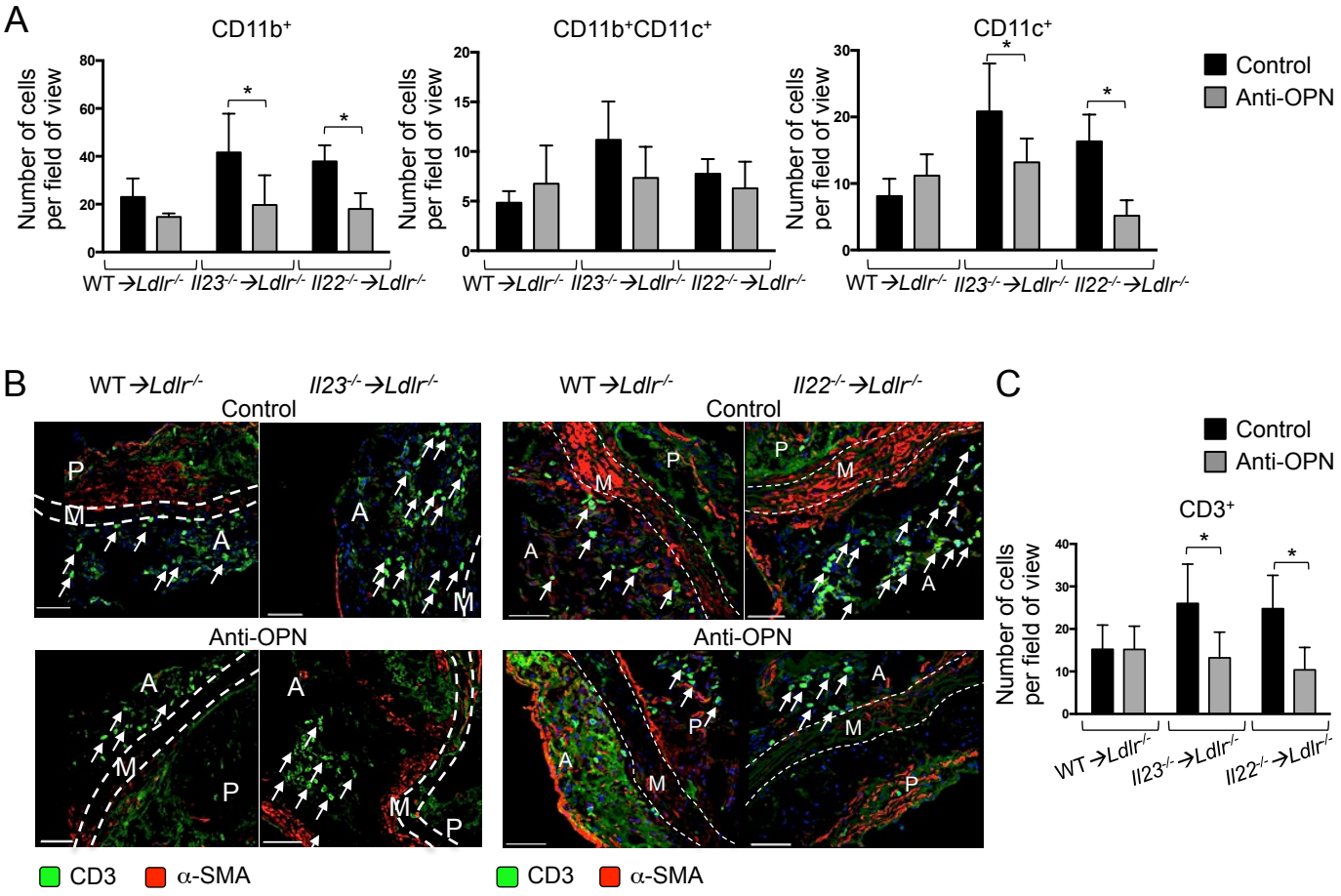
A
CD11b+
CD11b+CD11c+
CD11c+
Number of cells per field of view
Control
Anti-OPN
WT→Ldlr-/-
Il23-/-→Ldlr-/-
Il22-/-→Ldlr-/-
B
C
D
Spp1
Cd36
Fold change
Control
LPS
TMAO
LPS+TMAO
CD3
α-SMA

Figure S7.

Figure S7. OPN regulates immune cells accumulation in aortas of *Il23*$^{-/-}$→*Ldlr*$^{-/-}$ and *Il22*$^{-/-}$→*Ldlr*$^{-/-}$ mice. Related to Figure 6 and 7.

A. Quantification of CD11b^{+}, CD11b^{+}CD11c^{+} and CD11c^{+} cells in the aortic roots of WT→*Ldlr*$^{-/-}$, *Il23*$^{-/-}$→*Ldlr*$^{-/-}$ or *Il22*$^{-/-}$→*Ldlr*$^{-/-}$ mice treated with anti-OPN-antibody or control. **B, C.** Immunofluorescent analysis of aortic root sections. Representative images from 3 independent experiments. Localization of CD3^{+} T cells **(B)** and quantification of CD3^{+} T-cells **(C)** in aortic roots of WT→*Ldlr*$^{-/-}$, *Il23*$^{-/-}$→*Ldlr*$^{-/-}$ or *Il22*$^{-/-}$→*Ldlr*$^{-/-}$ mice treated with anti-OPN-antibody or control. Scale bar represents 50μm. A-adventitia, M-media, P-plaque. **D.** Relative gene expression in the explanted aortas of C57BL/6 mice treated with LPS and TMAO *ex vivo*. Gene expression was normalized to *RpL32* and then to gene expression in control group. Data are mean ±SEM from 2 independent experiments, *p<0.05, ***p<0.0001.